Geoscience Letters

RESEARCH LETTER

Open Access

Potential for tsunami detection via CCTV cameras in northeastern Toyama Prefecture, Japan, following the 2024 Noto Peninsula earthquake

Tomoki Shirai[1], Yota Enomoto[1], Keisuke Haga[1], Tatsuhiko Tokuta[1], Taro Arikawa[1*], Nobuhito Mori[2,3] and Fumihiko Imamura[4]

Abstract

This study explored closed-circuit television (CCTV) networks in northeastern Toyama Prefecture, Japan, as a new data source for tsunami detection following the 2024 Noto Peninsula earthquake. We analyzed CCTV footage and extracted time-series water level fluctuations at Yokoyama, Shimoiino, and Ekko. Spectral analysis of these waveforms revealed several long-period peaks (more than 100 s) in power spectral density (PSD), suggesting the presence of tsunami components. Notably, relatively large PSD peaks at approximately 5–10 min were observed at all CCTV locations in this study and at offshore wave observation points (Tanaka and Toyama). At Yokoyama, a maximum run-up of approximately 3 m was confirmed around 16:28. Although water level fluctuations at Shimoiino and Ekko were detected, identifying tsunami components proved challenging due to their small magnitude compared to other wave components. Despite these challenges, this study demonstrates the potential of CCTV networks for tsunami detection, and further research is needed to achieve real-time detection.

Keywords Tsunami detection, CCTV, Video footage analysis, Wave run-up, The 2024 Noto Peninsula earthquake

Introduction

Tsunamis pose significant risks to coastal areas, necessitating advancements in real-time detection and understanding of their generation mechanisms. Various technologies have been developed and utilized for observing sea-level changes to detect tsunamis, including GPS buoys (e.g., Kato et al. 2011) and seafloor pressure gauges, as well as networks like NOAA's PMEL DART (Deep-ocean Assessment and Reporting of Tsunamis) (Heidarzadeh and Satake 2013). In Japan, the Dense Ocean floor Network System for Earthquakes and Tsunamis (DONET) (Kaneda et al. 2015; Kawaguchi et al. 2015) and the S-net (Seafloor observation network for earthquakes and tsunamis along the Japan Trench) based on seismometers and pressure gauges (Kanazawa et al. 2016) have been established. Moreover, with advances in remote sensing technology, there has been discussion on the potential for using equipment other than offshore sensors for tsunami detection. Reports have highlighted the effectiveness of HF radar (Ogata et al. 2018) and satellite observations of minor sea-level changes in the mid-ocean caused by tsunamis (Koshimura et al. 2020). Video footage has also been reported as very effective for

*Correspondence:
Taro Arikawa
taro.arikawa.38d@g.chuo-u.ac.jp
[1] Department of Civil and Environmental Engineering, Chuo University, 1-13-27 Kasuga, Bunkyo-ku, Tokyo 112-8551, Japan
[2] Disaster Prevention Research Institute, Kyoto University, Gokasho, Uji, Kyoto 611-0011, Japan
[3] School of Engineering and Applied Sciences, Swansea University, Bay Campus, Swansea SA1 8EN, UK
[4] International Research Institute of Disaster Science, Tohoku University, 468-1 Aoba, Aramaki, Aoba-ku, Sendai, Miyagi 980-8572, Japan

tsunami analysis (e.g., McDonough-Margison et al. 2023). Despite these developments, observation networks capable of detecting tsunamis in coastal areas are still limited.

In Japan, an extensive network of Closed-Circuit Television (CCTV) cameras maintained by the Ministry of Land, Infrastructure, Transport, and Tourism (MLIT) provides constant monitoring across coasts, rivers, and roads. These cameras, part of a disaster prevention communications infrastructure, can transmit real-time images to local governments and TV stations during disasters, aiding in damage assessment. However, effectively leveraging this vast amount of video footage for operational purposes, such as tsunami detection, remains challenging (MLIT 2023). Demonstrations of the potential use of CCTV footage for detecting landslide-related disasters (Kinoshita et al. 2022) and observing river water levels (Sakai et al. 2015) have been conducted. The widespread deployment of coastal CCTV cameras illustrates their potential to enhance the coverage and resolution of the observational network for tsunami detection, complementing specialized offshore equipment. However, their effectiveness in actual tsunami events has yet to be thoroughly examined.

On January 1, 2024, the Noto Peninsula earthquake struck Ishikawa Prefecture, Japan, with its epicenter in the Noto region (37.495°N, 137.270°E, according to the provisional source fault model of the 2024 Noto Peninsula Earthquakes by Geospatial Information Authority of Japan (GSI) as of January 15, 2024), reaching a magnitude of Mw 7.5 (Japan Meteorological Agency (JMA), https://www.data.jma.go.jp/svd/eew/data/mech/fig/world20240101161000000N373000E13712000000076.html, last accessed February 10, 2024). The ensuing tsunami led to approximately 190 ha of flooding in Suzu City, Noto Town, and Shika Town, among others (Damage and Response to the 2024 Noto Peninsula Earthquake (58th Report) by MLIT 2024). However, reports of the tsunami around the northeastern part of Toyama Prefecture are limited due to a lack of tsunami observations. Therefore, this study analyzed and tried to extract tsunami waveforms and run-up height information from multiple CCTV footage installed in the northeastern part of Toyama Prefecture (Fig. 1).

The ultimate goal of utilizing CCTV cameras for tsunami detection in this study is twofold. Firstly, CCTV cameras function as a means for real-time monitoring and early warning, complementing traditional tsunami detection methods that heavily rely on offshore equipment. By analyzing waveforms and run-up heights from CCTV footage, we can enhance the accuracy and timeliness of tsunami alerts, thereby supporting prompt evacuation efforts. Secondly, the data collected from CCTV cameras facilitates detailed post-tsunami assessments, enabling a thorough analysis of the tsunami's impact and the effectiveness of existing disaster prevention measures. These approaches are expected to strengthen immediate tsunami response measures as well as contribute to the formulation of long-term tsunami disaster prevention strategies. The initial findings reported in this paper can support the feasibility of the aforementioned tsunami detection technology using CCTV cameras, paving the way for future advancements in this critical field.

Method

Field surveys and definition of transects in footage

Figure 2 illustrates the process employed in this method. Shoreline changes were observed at three CCTV locations—Yokoyama, Shimoiino, and Ekko—especially near recognizable landmarks such as stairs, which were chosen for elevation measurements in this study. We conducted onsite elevation surveys using the Real Time Kinematic (RTK) measurement method (with a SOKKIA GSX2 GNSS Receiver) and a Leica DISTO™ S910 laser rangefinder for shoreline measurements. Subsequently, transects within the scope of the footage were delineated (Fig. 3). In a pre-processed image (see "Method for extracting shoreline temporal changes from images" section), transects were assumed to be linear. Elevation information was then required to estimate wave run-up heights from the footage. Here, we posited that elevation z is uniquely determined by pixel position ($z = f(x, y(x))$), adopting a linear (for Shimoiino and Ekko) or quadratic (for Yokoyama) relationship between the observed z and the corresponding x on the transect. Assuming that lines connecting points with identical z -values across two "real" transects consistently share the same elevation z, and considering a flat slope, an estimated z for any pixel position (x, y) between the two transects was calculated. By creating multiple "virtual" transects between the "real" transects and averaging the shoreline position change extracted from several effective transects, we aimed to diminish noise in shoreline extraction and derive more reliable waveforms.

Method for extracting shoreline temporal changes from images

For the first step in Fig. 2a, the CCTV footage was decomposed frame by frame. The original footage has a frame rate of 29.97 fps (frames per second) and a frame size of 1920 by 1080. No projective transformation of the images was performed to analyze the images centered on the calibrated segments. The time averaging 29 frames, corresponding to about 1 s, was taken to reduce data processing costs and noise for edge detections. As shown in Fig. 3, frames without averaging and 0.1 s image average have too much noise

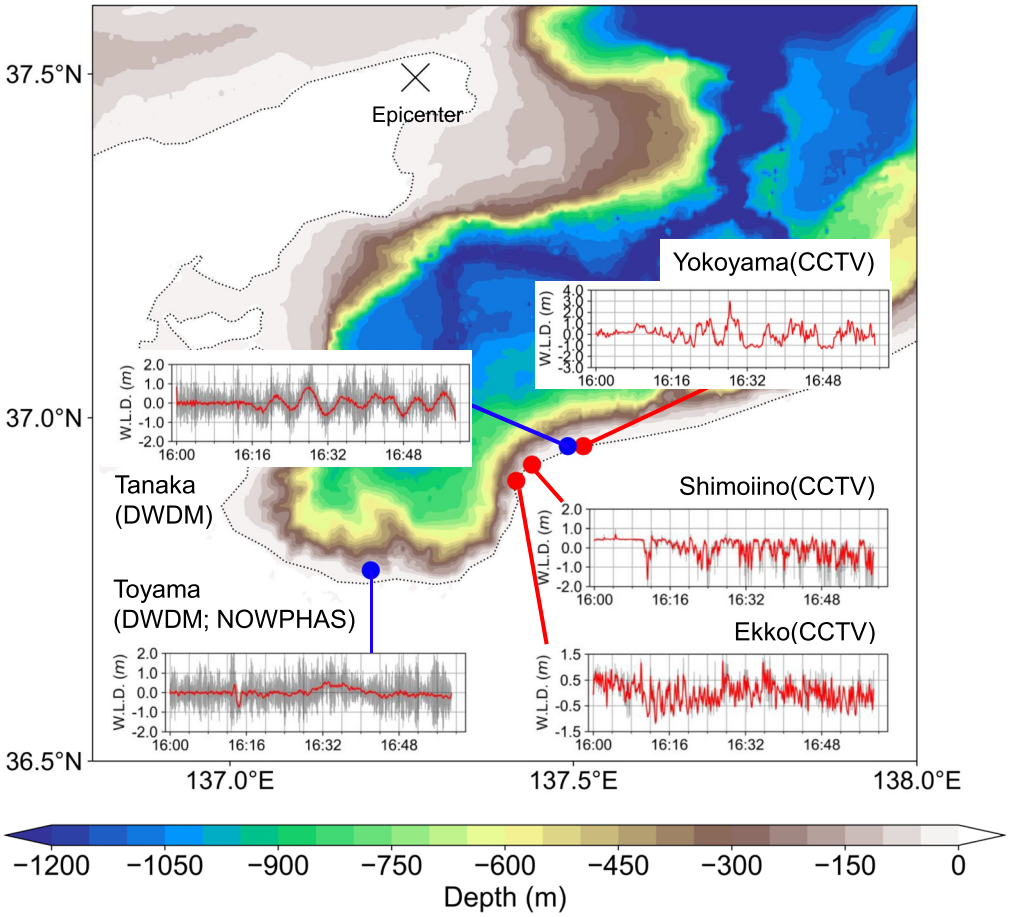

Fig. 1 Locations of the CCTV cameras used in this study and an overview of the observed or extracted water level deviations (WLD). Red dots indicate the locations of the CCTV cameras, and blue dots represent offshore wave observation (DWDM: Doppler-type Wave Directional Meter, NOWPHAS: Nationwide Ocean Wave information network for Ports and HArbourS) points. To extract the tsunami component, a low-pass filter with a cutoff period of 20 s was applied to the original extracted or observed waveforms (grey line), resulting in an approximation (red line). The background map displays color shading for water depth with data obtained from the GEBCO_2023 Grid. The "Epicenter" (latitude 37.4950, longitude 137.2700) is also marked

on the water surface due to edge detection (details of the edge detection are mentioned later). On the other hand, taking a 10–100 s time-averaging for the image reduces the noise. Still, it reduces the number of edge points detected, so continuous time-series data may not be obtained in situations where the image intensity difference is negligible. Therefore, we tried several image averaging intervals here and selected the 1-s averaged image balanced between relatively low noise and high stability of shoreline detection (Fig. 3). These averaged images were then trimmed to the portion used for analysis and converted to grayscale (image intensity values).

Then, for the second step in Fig. 2a, shoreline detection was performed by using the Canny edge detector (Canny 1986) for edge detection. The Canny Detector is widely regarded as one of the most popular algorithms for edge detection in gray images (Jing et al. 2022).

The OpenCV library was implemented in Python (https://docs.opencv.org/3.4/da/d5c/tutorial_canny_detector.html, last accessed February 10, 2024).

For the determination of the final shoreline position (the third step in Fig. 2a), several filtering steps were applied to the edge detection results:

1. Edges above a certain elevation (Max Elevation) were removed, which the shoreline could not have reached.
2. Remove edges detected at the same position above a threshold elevation a certain number of times to remove repetitive noise (e.g., lines detected on stairs). This condition is applied with a minimum elevation

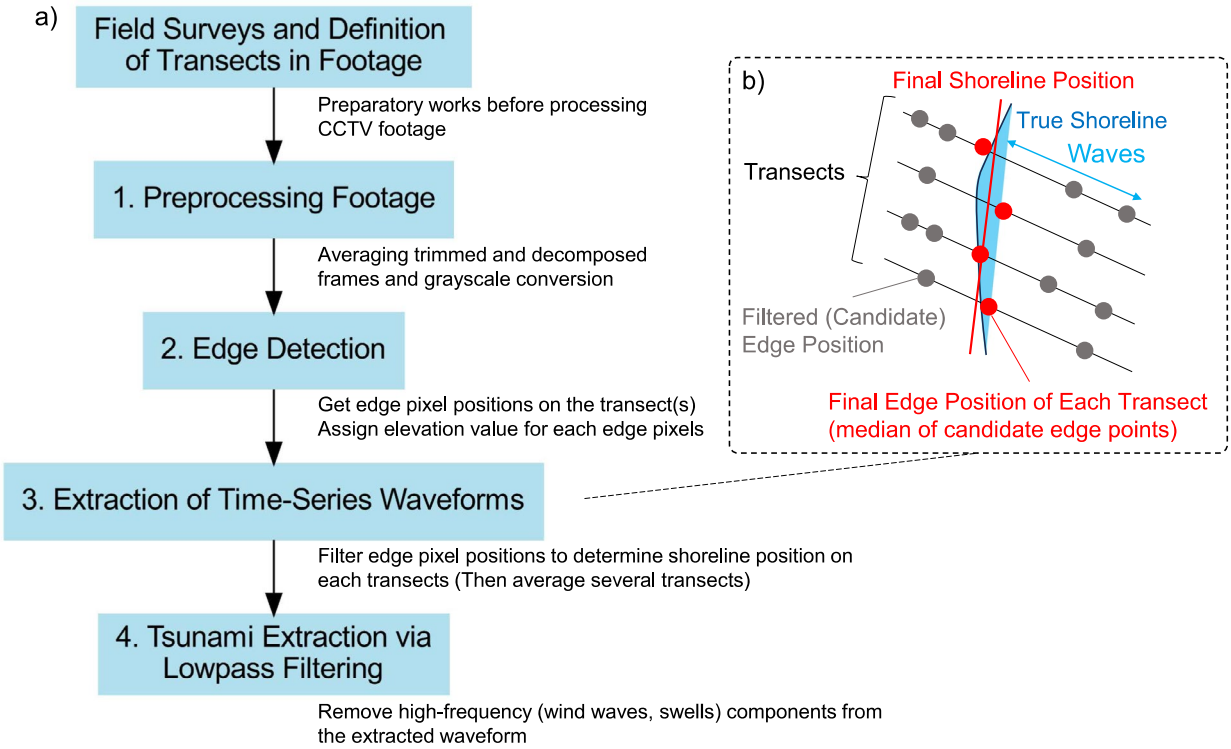

Fig. 2 **a** Methodology flowchart for this study. **b** A conceptual diagram of the method used to filter out noisy edges from the edge detection results and to determine the "Final Shoreline Position" in the step 3 of (**a**)

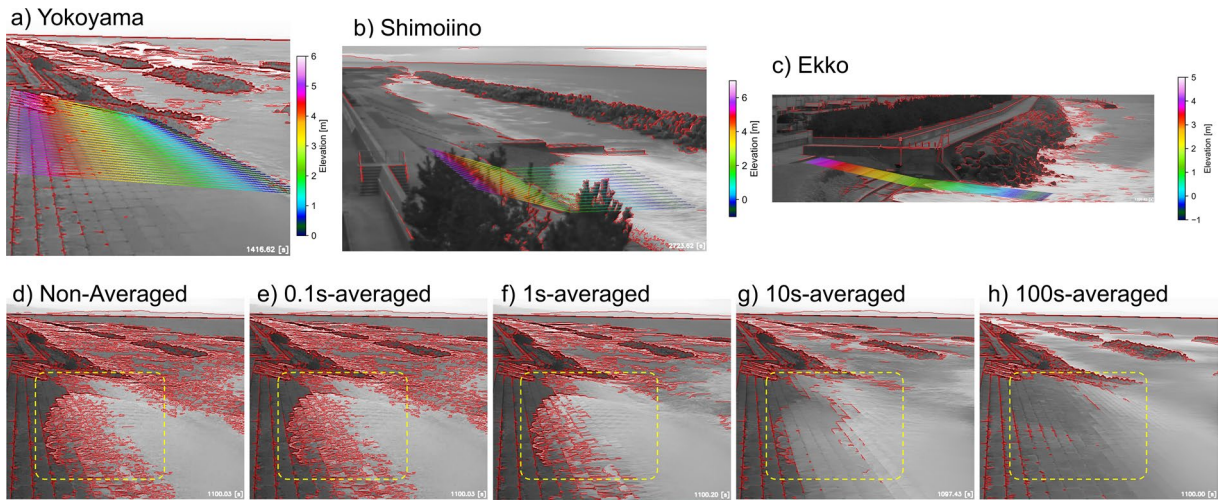

Fig. 3 Panels (**a**–**c**) display the transects and elevation distributions at Yokoyama, Shimoiino, and Ekko, respectively (for details on transects selected, see Supplementary Material Text S1). Panel **d** is an example of the original (simply trimmed) frame, and panels **e**–**h** are averaged images from around 16:28, when the maximum run-up occurred at Yokoyama. The red lines in the images represent the edges detected by the Canny Edge Detector. In the yellow frames in panels (**d**–**h**), variations in the density of edge pixels are observable

(Min Elevation) set to avoid erasing the minor water level fluctuations around the average shoreline position.

3. For noise not removed by steps 1 and 2, a sliding window was set as necessary, treating all data points within this window (e.g., size 5) as belonging to the same timestamp. This process reduces the chance of local noise (e.g., changes in luminance values after inundation) being mistakenly detected as the shoreline position, thereby making the process more robust.

Finally, the median of the remaining edges (elevations) at each timestamp was adopted as the shoreline position for that time. As shown in Fig. 2b, averaging the time-series waveforms obtained from multiple transects helped offset noise effects and extract robust time-series waveforms (for the parameters in the above processes, please refer to the Supplementary Material Table S1). Afterward, the time-series data were interpolated at 1-s intervals, regarding the image at 16:00:00 as the zero point. To validate the time-series data extracted, we compared their waveforms and spectral characteristics with the wave observations at Tanaka and Toyama (indicated by blue dots in Fig. 1). Spectral analysis was conducted using the Welch method from the scipy.signal library (version 1.11.4), implemented in Python. We primarily used the default parameters of the library to ensure the reproducibility of the analysis. For detailed information on the method and its default parameters, please refer to the SciPy documentation (https://docs.scipy.org/doc/scipy/reference/generated/scipy.signal.welch.html, last accessed April 20, 2024). Data sampling frequencies were set at 1 Hz for CCTV and 2 Hz for DWDM observations, covering the analysis period from 16:00 to 16:59. Given the specific challenges of detecting tsunami-related components within this limited dataset, the window length for spectral analysis was set equal to the data length. Additionally, to eliminate the influences of wind waves and swells from the full-time series, a fourth-order Butterworth low-pass filter, also from the SciPy library, was employed (the fourth step in Fig. 2a).

Results and discussion

Extraction results of waveforms and comparison of spectral characteristics

In the power spectral density (PSD) analysis (Fig. 4), Yokoyama and Tanaka exhibit the remarkably similar shape of the PSD distributions (e.g., 100–200 s, 200–300 s, 400–500 s, and 885 s), with the highest PSD peaks at Yokoyama was 393 s, and Tanaka was 443 s. The peak at 885 s is unique and not observed at other locations, while a common spectral peak at 400–500 s is present in all locations. Ekko displays a peak at 590 s, but a peak

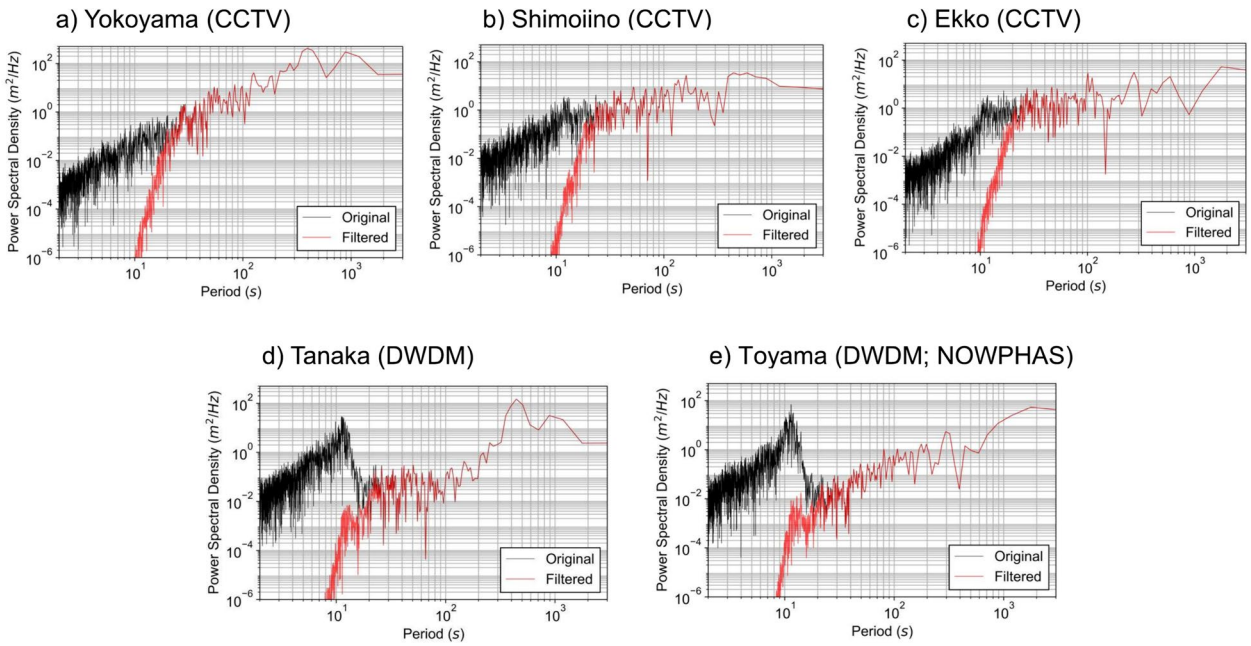

Fig. 4 Power spectral density analysis results for each location. Here, "Original" refers to the PSD for waveforms obtained from Step 3 in Fig. 2a for CCTV, which are at a 1-s interval, and for DWDM, it refers to the PSD for observed raw waveforms at a 0.5-s interval. "Filtered" denotes the result of applying a 20 s low-pass filter, which mitigates the effects of wind waves and swells to the "Original", which for CCTV, corresponds to the outcome of Step 4 in Fig. 2a

at 272 s is also notably prominent, resembling the trend in Toyama, where 295 s is predominant. This similarity might be attributed to Ekko's proximity to Toyama Bay, closer than any other location. Furthermore, all locations show relatively large peaks within the 100–200 s range. Such consistency suggests that approximately 100–200 s, 200–300 s, 400–500 s, and 885 s may represent the spectral characteristics of this tsunami event in the northeastern part of Toyama Prefecture.

For waveforms, only Yokoyama's result is mentioned due to space constraints. In Fig. 5, the extracted time-series waveforms are represented by a gray line. In contrast, a red line depicts the low-pass filtered waveform with a 20-s cutoff period determined from spectral analysis (see Fig. 4). Both the original and the low-pass filtered waveforms for Shimoiino and Ekko are presented in Fig. 1. It should be noted that the mean water level, calculated from the overall analysis window from 16:00 (start of the analysis) to 16:59 (end of the analysis), was set to zero.

For Yokoyama, significant peaks in water level deviation were detected in the filtered waveform at approximately 16:21, 16:24, 16:28 (with the lowpass-filtered maximum run-up height above the mean water level being 2.98 m), 16:36, 16:41, 16:43, and 16:53. Tanaka is a location situated approximately 2 km away from Yokoyama, observed from a position just offshore. The peaks in the filtered waveforms at Tanaka around 16:21, 16:28 (with the maximum wave height being 1.37 m), 16:34, 16:42, 16:51, and 16:56 align well with the times of significant water level deviations observed in Yokoyama. Yokoyama exhibits a slightly delayed phase by several tens of seconds, especially noticeable until around 16:40 compared to Tanaka. This delay is reasonable, given that Tanaka is located slightly offshore, while observations in Yokoyama are made from the shoreline at the coastal dike. Moreover, gentler sea surface elevations in Toyama were observed around 16:30–40. Given the Toyama wave observation station is located further south from Yokoyama and Tanaka and further from the fault, it suggests

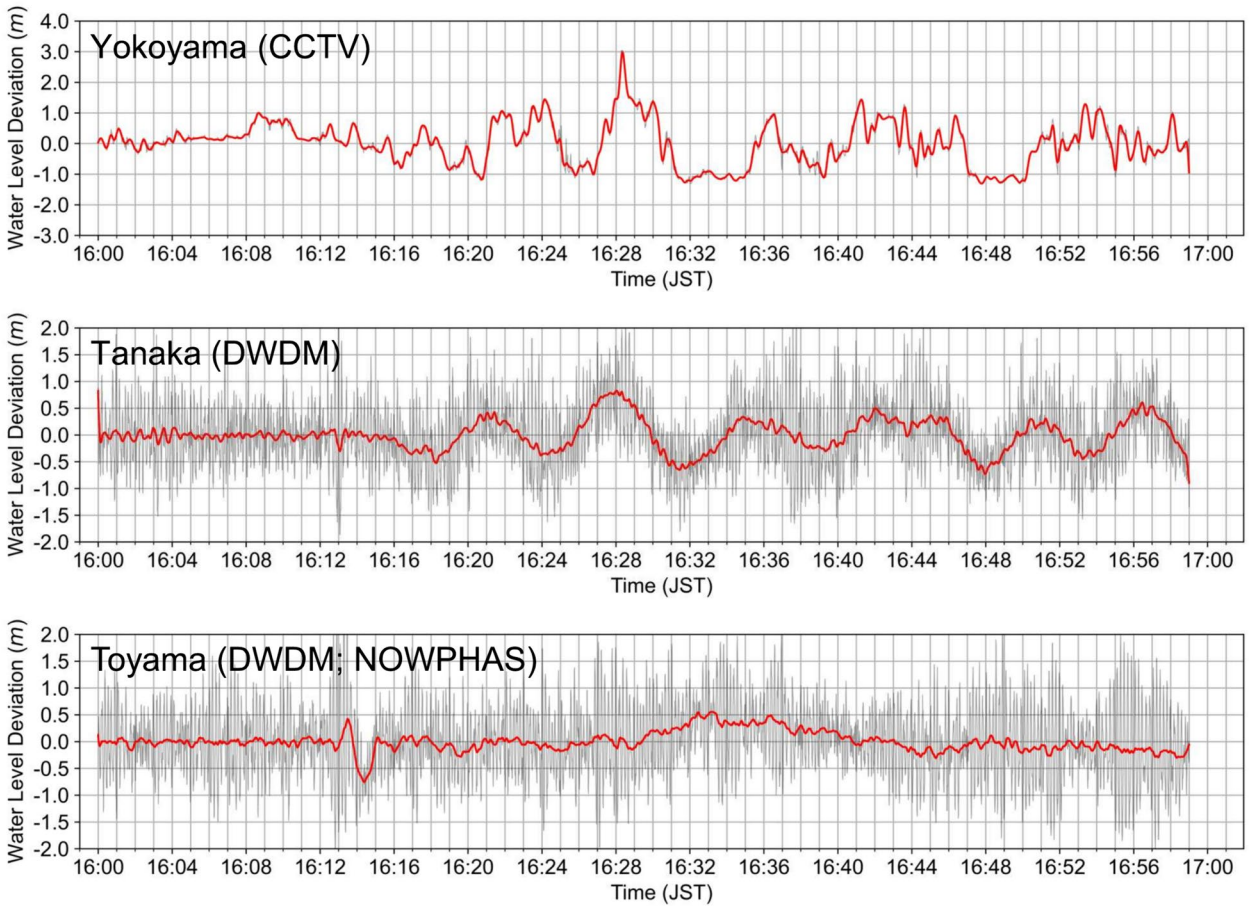

Fig. 5 Waveforms for Yokoyama, Tanaka, and Toyama. Consistent with Fig. 4, grey lines indicate "original" waveforms, and red lines represent "filtered" waveforms

that these fluctuations could be attributed to tsunami components.

Including Shimoiino and Ekko, significant deviations in water levels were observed in the northeastern part of Toyama Prefecture (excluding Toyama) around 16:27–28 and 16:33–36, as well as before and after these times. While the fault in the northern part of the Noto Peninsula, which triggered the Mw 7.5 earthquake, is identified as a potential wave source, the relatively early arrival of the wave peak before 16:27–28 suggests that this fault alone may not fully account for the observations. A numerical simulation using the fault model from the GSI (2024) (Supplementary Material Figure S1) also suggest that additional factors, such as landslides, might have contributed to these relatively early waves. It should be noted that while the results from Fujii and Satake (2024) offer preliminary support for the simulation, the fault model remains uncertain and necessitates further detailed validation.

Limitations of the presented method and potential for real-time tsunami detection

Overcoming obstacles for real-time tsunami detection is crucial, with the primary challenge being the differentiation of tsunami-induced waveform peaks from other disturbances. For instance, in Yokoyama, distinct peaks are observed at 16:28 and 16:36, among others at 16:18–16:21, and even before the earthquake. Distinguishing tsunami signals amidst noisy waveforms in Shimoiino and Ekko proves difficult with the current method. Typically, two types of noise exist: wave-originated errors (e.g., effects of topography, wave setup, or wave reflections) and inaccuracies in shoreline detection. The latter includes data affected by seismic motion blurring, observed explicitly in Shimoiino and Ekko around 16:10 (Fig. 1) (especially, it should be noted that a sharp negative WLD (water level deviation) observed around 16:10 in Shimoiino was noise caused by the camera angle being shaken by the earthquake tremors, leading to the failure of shoreline detection. Therefore, it is important to clarify that an actual decrease in WLDs, as would appear in time-series waveforms in Fig. 1, did not occur).

For the former, our study's limited pre-earthquake data (16:00–16:10) restricted a comprehensive analysis of non-tsunami conditions and removing these noises. For the latter, post-inundation wet conditions at Yokoyama after the 16:28 run-up improved shoreline detection (with roughly a 0.5 m error margin as a common measure), yet pre-16:28 low WLDs frequently caused edge detection failures, indicating potential errors of up to around 1 m.

It is worth noting that this study emphasized developing detection methods that are as versatile as possible, focusing on a balance between minimizing errors and ensuring adaptability across various sites as a prototype. However, the applicability to other sites has not been verified, and this method may not necessarily be optimal for addressing the above trade-offs, necessitating further investigation.

Conclusion

This study analyzed CCTV footage from northeastern Toyama Prefecture to identify potential tsunami signatures following the Noto Peninsula earthquake on January 1, 2024. The analysis revealed wave run-up time-series waveforms, including long-period (especially 5–10 min) components suggestive of possible tsunamis. Clear run-up peaks were identified in Yokoyama around 16:28 with a maximum run-up height from the mean water level of 2.98 m, aligning with offshore wave observations at Tanaka, demonstrating spectral and waveform consistency for these long-period components. In Shimoiino and Ekko, components suggestive of potential tsunamis were detected, with spectral characteristics similar to those observed in other locations (Yokoyama, Toyama (DWDM, NOWPHAS), and Tanaka). However, the low magnitude of these components in Shimoiino and Ekko made it challenging to distinguish them from other wave components with the current method. This indicates the need for further research to refine detection methods and advance toward real-time tsunami monitoring to enable automatic detection of tsunami signals, while acknowledging that the current technique still relies on some subjective interpretation.

Abbreviations

CCTV	Closed-circuit television
GSI	Geospatial Information Authority of Japan
MLIT	Ministry of Land, Infrastructure, Transport, and Tourism
NOWPHAS	Nationwide Ocean Wave information network for Ports and HArbourS
DWDM	Doppler-type Wave Directional Meter

Supplementary Information

The online version contains supplementary material available at https://doi.org/10.1186/s40562-024-00343-9.

Supplementary Material 1.

Acknowledgements

CCTV footage and wave observation data (Tanaka) used in this study were provided by the Ministry of Land, Infrastructure, Transport and Tourism, Hokuriku Regional Development Bureau. The NOWPHAS (Nationwide Ocean Wave information network for Ports and HArbourS) data (Toyama) were observed and provided by the Ports and Harbours Bureau, Ministry of Land, Infrastructure, Transport and Tourism.

Author contributions

TS analyzed CCTV footage and was a major contributor in writing the manuscript. TS, YE, and TA conducted the field survey and contributed to the

conception. TT and KH conducted numerical simulations and verified the validity of results compared with the processed CCTV footage. TA, FI, and NM supervised and revised the manuscript. All authors read and approved the final manuscript.

Funding
None.

Availability of data and materials
A sample code for CCTV footage analysis used in this study will be made available on the author's GitHub page (https://github.com/Chuocoastlabo) by next summer in Japan. The CCTV footage cannot be made available immediately due to the need for permission from the provider.

Declarations

Competing interests
The authors declare that they have no competing interests.

Received: 2 March 2024 Accepted: 21 May 2024
Published online: 05 June 2024

References

Canny J (1986) A computational approach to edge detection. IEEE Trans Pattern Anal Mach Intell PAMI 8(6):679–698. https://doi.org/10.1109/TPAMI.1986.4767851

Fujii Y, Satake K (2024) Slip distribution of the 2024 Noto Peninsula earthquake (MJMA 7.6) estimated from tsunami waveforms and GNSS data. Earth Planets Space 76:44. https://doi.org/10.1186/s40623-024-01991-z

Geospatial Information Authority of Japan (2024) Source fault model as of January 15, 2024. https://www.gsi.go.jp/common/000254837.pdf. Accessed 10 Feb 2024

Heidarzadeh M, Satake K (2013) Waveform and spectral analyses of the 2011 Japan tsunami records on tide gauge and DART stations across the Pacific Ocean. Pure Appl Geophys 170:1275–1293. https://doi.org/10.1007/s00024-012-0558-5

Jing J, Liu S, Wang G, Zhang W, Sun C (2022) Recent advances on image edge detection: a comprehensive review. Neurocomputing 503:259–271. https://doi.org/10.1016/j.neucom.2022.06.083

Kanazawa T, Uehira K, Mochizuki M, Shinbo T, Fujimoto H, Noguchi S, Kunugi T, Shiomi K, Aoi S, Matsumoto T, Sekiguchi S, Okada Y (2016) S-net project, cabled observation network for earthquakes and tsunamis. Presented at SubOptic 2016, Dubai, 18–21 April, Abstract WE2B-3

Kaneda Y, Kawaguchi K, Araki E, Matsumoto H, Nakamura T, Kamiya S, Takahashi N (2015) Development and application of an advanced ocean floor network system for megathrust earthquakes and tsunamis. In: Favali P, Beranzoli L, De Santis A (eds) SEAFLOOR OBSERVATORIES: A New Vision of the Earth from the Abyss. Springer, Berlin, pp 643–662. https://doi.org/10.1007/978-3-642-11374-1_25

Kato T, Terada Y, Nishimura H, Nagai T, Si K (2011) Tsunami records due to the 2010 Chile Earthquake observed by GPS buoys established along the Pacific coast of Japan. Earth Planets Space 63(6):e5–e8. https://doi.org/10.5047/eps.2011.05.001

Kawaguchi K, Kaneko S, Nishida T, Komine T (2015) Construction of the DONET real-time seafloor observatory for earthquakes and tsunami monitoring. In: Favali P, Beranzoli L, De Santis A (eds) SEAFLOOR OBSERVATORIES: A New Vision of the Earth from the Abyss. Springer, Berlin, pp 211–228. https://doi.org/10.1007/978-3-642-11374-1_10

Kinoshita A, Kaihara S, Ibuka S, Kitamoto G, Nakaya H, Kanazawa A, Yamakoshi T (2022) Development of the disaster detection system by brightness difference of CCTV images. Adv River Eng 28:13–18. https://doi.org/10.11532/river.28.0_13. (**In Japanese**)

Koshimura S, Moya L, Mas E, Bai Y (2020) Tsunami damage detection with remote sensing: a review. Geosciences 10(5):177. https://doi.org/10.3390/geosciences10050177

McDonough-Margison C, Hinchliffe G, Petterson MG (2023) Analysing civilian video footage for enhanced scientific understanding of the 2011 Tohoku Earthquake and Tsunami, Japan, with implications for PNG and Pacific Islands. Geosciences 13(7):203. https://doi.org/10.3390/geosciences13070203

Ministry of Land, Infrastructure, Transport and Tourism (2023) Telecommunications technology vision 4. https://www.mlit.go.jp/report/press/content/001594487.pdf. Accessed 10 Feb 2024

Ministry of Land, Infrastructure, Transport and Tourism (2024) Damage and Response to the 2024 Noto Peninsula Earthquake (58th Report), https://www.mlit.go.jp/common/001720916.pdf. Accessed 10 Feb 2024

Ogata K, Seto S, Fuji R, Takahashi T, Hinata H (2018) Real-time tsunami detection with oceanographic radar based on virtual tsunami observation experiments. Remote Sens 10(7):1126. https://doi.org/10.3390/rs10071126

Sakai K, Yamada S, Watabe K, Umeda S, Haishima S, Yorozuya A (2015) Research for improvement of water level measurement accuracy using a CCTV camera. Adv River Eng 21:61–66. https://doi.org/10.11532/river.21.0_61. (**In Japanese**)

Publisher's Note